



# NIH Public Access

## Author Manuscript

Biochemistry. Author manuscript; available in PMC 2013 March 27.

Published in final edited form as:  
*Biochemistry*. 2012 March 27; 51(12): 2378–2389. doi:10.1021/bi300106p.

## Linking energy production and protein synthesis in hydrogenotrophic methanogens

Javin P. Oza<sup>1</sup>, Kevin R. Sowers<sup>3</sup>, and John J. Perona<sup>1,2,\*,#</sup>

<sup>1</sup>Interdepartmental Program in Biomolecular Science and Engineering, University of California, Santa Barbara, CA 93106-9510

<sup>2</sup>Department of Chemistry and Biochemistry, University of California, Santa Barbara, CA 93106-9510

<sup>3</sup>Department of Marine Biotechnology, Institute of Marine and Environmental Technology, University of Maryland Baltimore County, Baltimore MD 21202

### Abstract

Hydrogenotrophic methanogens possessing the hydrogen-dependent dehydrogenase Hmd also encode paralogs of this protein whose function is poorly understood. Here we present biochemical evidence that the two inactive Hmd paralogs of *Methanocaldococcus jannaschii*, HmdII and HmdIII, form binary and ternary complexes with several components of the protein translation apparatus. HmdII and HmdIII, but not the active dehydrogenase Hmd, bind with micromolar binding affinities to a number of tRNAs, and form ternary complexes with tRNA<sup>Pro</sup> and prolyl-tRNA synthetase (ProRS). Fluorescence spectroscopy experiments also suggest that binding of HmdII and ProRS involves distinct binding determinants on the tRNA. These biochemical data suggest the possibility of a regulatory link between energy production and protein translation pathways that may allow a rapid cellular response to altered environmental conditions.

Methane generation in Earth's biosphere is restricted to a class of microbes within the domain *Archaea*: the methanogens. A limited number of one and two-carbon substrates support the growth of these organisms, including formate, methanol, methylamines, and acetate.<sup>1,2</sup> Most methanogens are also capable of hydrogenotrophic growth from molecular hydrogen and carbon dioxide, converting these substrates to methane and water. At typical environmental partial pressures of H<sub>2</sub>, the available free energy gradient is such that less than one mole of ATP is synthesized per mole of methane formed.<sup>3,4</sup> The metabolism of hydrogenotrophic methanogens thus operates near to thermodynamic limits, giving rise to a variety of molecular adaptations that function to conserve energy. While some adaptations are found generally among the *Archaea*,<sup>5</sup> others are more specific: methanogens that are obligate hydrogenotrophs are exquisitely sensitive to concentrations of H<sub>2</sub> and of certain transition metal ions, and transcribe distinct isozymes at specific steps in the methanogenesis pathway in response to changes in the environmental abundances of these substances.<sup>6</sup>

\*Corresponding author. Tel. 503-725-2426; perona@pdx.edu.

#Present address: Department of Chemistry, Portland State University, PO Box 751, Portland OR 97207, and Department of Biochemistry and Molecular Biology, Oregon Health & Sciences University, 3181 SW Sam Jackson Park Road, Portland, OR 97239.

### Supporting Information

An example of a SEC-MALS analysis (Figure S1), a steady-state fluorescence anisotropy experiment showing complex formation between ProRS and HmdII (Figure S2), experiments showing ternary complex formation by fluorescence polarization in which the order of titration is reversed (Figure S3), an experiment showing the effects of Hmd proteins on active site titrations of ProRS (Figure S4), and a depiction of single-turnover kinetics (Figure S5) are each provided together with figure legends. This material is available free of charge via the Internet at <http://pubs.acs.org>.

Methanogenesis from H<sub>2</sub> and CO<sub>2</sub> comprises a seven-step pathway that is coupled to the generation of membrane proton and sodium gradients used for ATP synthesis. The fourth step in the pathway, in which 5,10-methenyltetrahydromethanopterin (methenyl-H<sub>4</sub>MPT) is reversibly converted to 5,10-methylene-H<sub>4</sub>MPT, is mediated by several enzymes and is a particular focus of environmental regulation.<sup>7–10</sup> Under conditions of low H<sub>2</sub> and high nickel concentrations, this step is catalyzed by the coenzyme F<sub>420</sub>-dependent N<sup>5,N<sup>10</sup></sup>-methylene tetrahydromethanopterin dehydrogenase (Mtd).<sup>11–13</sup> The oxidized F<sub>420</sub> generated in this reaction is in turn reduced to H<sub>2</sub>-F<sub>420</sub> by the nickel-containing F<sub>420</sub>-dependent hydrogenases Frh and Fru.<sup>14</sup> However, when nickel concentrations are low or when H<sub>2</sub> is not limiting, the interconversion of 5,10-methenyl-H<sub>4</sub>MPT and 5,10-methylene-H<sub>4</sub>MPT is catalyzed by the H<sub>2</sub>-forming N<sub>5,N<sup>10</sup></sub>-methylene-H<sub>4</sub>MPT dehydrogenase (Hmd), which directly uses molecular H<sub>2</sub> as the reductant.<sup>7–8,12,15–16</sup> Nickel limitation also gives rise to an alternative pathway for regeneration of F<sub>420</sub>-H<sub>2</sub>. Under these conditions, Hmd and Mtd function in a concerted manner to reduce F<sub>420</sub>: Hmd operates in the direction of 5,10-methylene-H<sub>4</sub>MPT synthesis, while Mtd operates in the reverse direction.<sup>17</sup>

Hmd is a nickel-independent, iron-sulfur cluster-free [Fe]-hydrogenase that contains a unique iron-guanlypyridinol cofactor (FeGP) in its active site.<sup>18–21</sup> The enzyme is a homodimer of 38 kD molecular weight subunits, binds two molecules of FeGP, and possesses a uniquely structured C-terminal helical bundle forming a major portion of the dimer interface region. The 250 residue N-terminal domain folds into a canonical Rossmann six-stranded parallel β-sheet.<sup>21</sup> The N- and C-termini of the monomers are intertwined, generating additional intersubunit contacts between the C-terminal domain and a portion of the opposing N-terminal domain that is relatively distant from the catalytic site.

Most methanogens possessing Hmd also possess one or two paralogs of the protein, as first identified in the genomes of *Methanocaldococcus jannaschii* JAL-1 (*Mj*) and *Methanobacterium thermoautotrophicus* ΔH (*Mt*).<sup>22,23</sup> The protein products of these paralogous genes, HmdII and HmdIII, are expressed in *Mt* cells.<sup>7</sup> The HmdII and HmdIII paralogs share approximately 80% amino acid sequence identity with each other, but are only about 20% identical to Hmd.<sup>24</sup> Interestingly, while it appears that neither paralog present in *Mt* possesses the catalytic activity characteristic of Hmd,<sup>7</sup> heterologously produced HmdII from *Mj* is able to compete with active Hmd for cofactor binding.<sup>20</sup> Further, the three Hmd proteins in *Mt* are differentially regulated in response to environmental cues.<sup>7</sup> When nickel concentrations are limiting, Hmd is induced but the expression of both HmdII and HmdIII is unaffected. In contrast, there is no change in Hmd expression when low concentrations of H<sub>2</sub> limit growth. However, under these conditions, the HmdII protein is present at elevated levels while the amount of HmdIII decreases.<sup>7</sup> The data suggest that, at least under some environmental conditions, the three Hmd proteins in *Mt* may have distinct functions *in vivo*.

Some insight into a possible function of the paralogs was offered by the finding that HmdII copurifies with prolyl-tRNA synthetase (ProRS) from *Mj* cell lysates.<sup>25,26</sup> This suggested that the Hmd paralogs might play a regulatory role by linking the energy generation and protein synthesis machineries of the cell. ProRS functions as one of the approximately twenty distinct cellular tRNA synthetase enzymes, which each covalently attach a particular coded amino acid to tRNAs of a matching isoaccepting group, thus providing cognate aminoacyl-tRNA for ribosomal protein synthesis. In *Mt*, ProRS associates into a complex with elongation factor 1A (EF-1A) and two other tRNA synthetases, possibly to increase translational efficiency *in vivo*.<sup>27,28</sup> In addition to their canonical role, accumulating evidence shows that tRNA synthetases function in diverse other capacities, including cell signaling, translational silencing, and activation of transcription.<sup>29</sup> Indeed, in bacteria, tRNA synthetases are central to the regulatory control of gene expression in response to nutrient

limitation.<sup>30</sup> Of further possible significance is the finding that the unusual phosphoseryl- and pyrrolylsyl-tRNA synthetases (SepRS; PylRS) are found only in methanogens or highly related archaea.<sup>31,32</sup> This suggests that particular aspects of cellular physiology related to methanogenesis may be linked to the machinery of protein synthesis.

Preliminary *in vitro* experiments suggested that *Mj* HmdII binds ProRS with physiologically relevant affinity, and that this paralog may also associate separately with tRNA.<sup>26</sup> To more thoroughly explore the nature of the interactions between the paralogs and components of the translational apparatus, we have now examined in detail the interactions of all three Hmd proteins with *Mj* tRNAs and ProRS *in vitro*. The new data demonstrate the formation of specific ternary protein-RNA complexes that include ProRS and either HmdII or HmdIII, but not Hmd. The observed specificities of tRNA and ProRS complex formation among the three Hmd proteins are readily correlated with their divergent tertiary structures, offering support for the notion that methanogenesis from H<sub>2</sub> and CO<sub>2</sub> is metabolically linked to protein synthesis. Interactions between components of the protein synthesis and methanogenesis pathways might contribute to a rapid physiological response to changing environmental conditions.

## MATERIALS AND METHODS

### Expression and Purification of Proteins

*Mj* genomic DNA was purchased from the American Type Culture Collection (ATCC 43067D-5) and used as template for the PCR amplification of the genes encoding *Mj*0715 (Hmd), *Mj*1338 (HmdII), and *Mj*0785 (HmdIII). The primers used were: 5'-AAACTGCATATGAAAATAGCAATCTTAGGAGCTG (forward primer) and 5'-CGCGGATCCTTATTCTCTTTGAGACATTA (reverse primer) for Hmd, 5'-GGGAATTCCATATGCGTAATATAAGAAAAA (forward primer) and 5'-CGCGGATCCTTAATGCTCAAATAATTCT (reverse primer) for HmdII, and 5'-AAACTGCATATGAAAATATCAATATATGGAGCTG (forward primer) and 5'-CGCGGATCCTTATTGAATAATTATTGAACCTT (reverse primer) for HmdIII. The reaction was carried out using 100 ng of *Mj* genomic DNA, 2 μM of each primer (forward and reverse), 250 μM dNTPs, 10× Pfu turbo reaction buffer and 2.5 U Pfu turbo DNA polymerase, at an annealing temperature of 51°C for 30 seconds and an extension time of 90 seconds per cycle for a total of 31 cycles. Amplicons were subsequently digested with NdeI and BamHI and cloned into pET16B, which provides a cleavable N-terminal His-tag, for expression in *Escherichia coli* Rosetta2(DE3) pLysS cells. The expression clone for *Mj* ProRS was the generous gift of Ya-Ming Hou.<sup>26</sup> Cells harboring plasmid expression constructs encoding *Mj* Hmd, HmdII, HmdIII or ProRS were grown at 37°C in Luria-Bertani (LB) medium with protein expression induced upon addition of isopropyl-β-d-thiogalactoside (IPTG) to a final concentration of 1 mM at OD<sub>600</sub> of 0.8. Cells were grown for an additional 6 hr at 37°C prior to harvesting by centrifugation. Cells were lysed by sonication and the enzymes purified with Ni-NTA resin (Qiagen) according to manufacturers' guidelines. This procedure provided robust yields in excess of 30 mg of 95% pure protein per liter of cells in each case. Purified protein was subsequently dialyzed into storage buffer comprised of 50 mM HEPES (pH 7.5), 100 mM NaCl, 20 mM KCl, 5 mM DTT, and 50% glycerol at -20C.

### Preparation of tRNAs

Wild type *Mj* tRNA<sup>Cys</sup>, *Mj* tRNA<sup>Leu(UAA)</sup>, *Mj* tRNA<sup>Lys</sup>, *Mj* tRNA<sup>Asp</sup> and *Mj* tRNA<sup>Pro(UGG)</sup> were transcribed from synthetic duplex DNA templates. The templates were each first synthesized from two overlapping synthetic oligodeoxyribonucleotides (purchased from IDT or from Fisher Operon; see Supplementary Information for sequences). Overlapping DNAs

were extended using Klenow fragment of *E. coli* DNA polymerase I, as described, and were recovered by ethanol precipitation.<sup>33</sup> *In vitro* transcription reactions were then performed as described.<sup>33</sup> Typically, 0.1 mg of DNA template was used in the transcription reaction to generate 1 mg of tRNA. tRNAs were purified by gel extraction and stored as ethanol precipitates or in purified water.

### Size exclusion chromatography coupled to multiangle light scattering

To determine molecular weights of ProRS, Hmd, HmdII, HmdIII and tRNA, size-exclusion chromatography in conjunction with multiangle static light-scattering (SECMALS) was employed.<sup>34</sup> One-hundred  $\mu$ l volumes of protein samples maintained at 3 mg/mL in a solution containing 50 mM HEPES (pH 7.5), 100 mM NaCl, 20 mM KCl, 10 mM MgCl<sub>2</sub>, and 5 mM DTT were first separated on a Wyatt WTC-030S5 size-exclusion column at a flow rate of 0.50 mL/min using a Waters 600 HPLC, and were then analyzed in-line by a UV/Vis spectrophotometer, a Wyatt miniDAWN TREOS light-scattering detector, and a Wyatt Optilab T-rEX refractive index detector. Prior to the experiments, the column running buffer, comprised of 50 mM HEPES (pH 7.5), 100 mM NaCl, 20 mM KCl, 10 mM MgCl<sub>2</sub>, and 5 mM DTT was sterile-filtered (0.20  $\mu$ m) and degassed for 10 min. The elution profile from the columns was recorded and analyzed with the Wyatt ASTRA software suite using bovine serum albumin (BSA) as standard. The stoichiometry of protein:RNA complexes in peak fractions, where relevant, was derived from measurements of the A<sub>260</sub>/A<sub>280</sub> ratio.<sup>35,36</sup> Separate runs comprising purified protein and RNA complexes, and complexes of defined stoichiometries, were conducted. dN/dC values for the tRNA<sup>Pro</sup> transcript and for the ProRS:tRNA<sup>Pro</sup> complex were determined as 0.193 and 0.1866, respectively.<sup>36</sup>

### Electrophoretic Mobility Shift Assays (EMSA)

tRNAs were radiolabeled at the 3'-internucleotide linkage by using the exchange activity of *E. coli* tRNA nucleotidyltransferase enzyme, as previously described.<sup>33,37</sup> Radiolabeled tRNAs were subsequently loaded onto BioSpin P-6 (BioRad) gel filtration columns to purify product from unincorporated label. Low concentrations of radiolabeled tRNAs (in the nanomolar range) were then refolded and incubated at ambient temperature for 30 min. with varying amounts of Hmd, HmdII or HmdIII (0–45  $\mu$ M dimers) in a buffer containing 10 mM HEPES (pH 7.5), 10 mM NaCl, 1.2 mM MgCl<sub>2</sub>, and 1 mM DTT. Complexes were then analyzed by PAGE on an 8% gel prepared with 0.5X TBE (Tris-Borate-EDTA - a buffer consisting of 90 mM Tris (pH 8.2), 90 mM boric acid, and 2 mM EDTA), and run at 4°C for 1 hour at 100 volts.<sup>38</sup> Gels were exposed to a phosphor screen overnight and imaged with a Typhoon imager (Molecular Dynamics). Bands corresponding to free and bound tRNAs were quantified using ImageQuant 5.2 and the data fit using GraphPad Prism.

### Steady-state Fluorescence Anisotropy

The *M. jannaschii* tRNA<sup>Pro</sup> transcript was site-specifically labeled at the 5'-end with fluorescein maleimide, as previously described.<sup>39,40</sup> Briefly, the gel-purified tRNA transcript was first treated with antarctic phosphatase (NEB) to dephosphorylate the 5'-terminus, which was then thiolated using the activity of T4 polynucleotide kinase (NEB) with ATP- $\gamma$ -S as the sulfur donor. Fluorescein-5-maleimide (AnaSpec) was subsequently incubated with the thiolated tRNA for 5'-labeling. ProRS was nonspecifically labeled with Alexafluor 488 tetrafluorophenyl ester (Invitrogen) according to manufacturer's guidelines. The labeling reaction was performed at pH 6.7 to provide specificity for the primary amine at the protein N-terminus as compared with side-chain labeling of lysine. Excess unincorporated label was removed by dialysis.

Binding experiments were conducted at 25°C under temperature-controlled conditions on a Perkin-Elmer LS55 luminescence spectrometer, in 50 mM HEPES (pH 7.5), 10 mM MgCl<sub>2</sub>,

100 mM NaCl, 20 mM KCl, 5 mM DTT.<sup>37,39,41</sup> For RNA-protein binding, the polarization of 5'-Fluorescein-tRNA<sup>Pro</sup> fluorescence was monitored as ProRS or Hmd proteins were titrated in. 5 nM labeled tRNA was first refolded and introduced to a buffer-containing quartz micro-cuvette. Labeled tRNA was allowed to incubate with the added protein for 5 minutes at each titration point, followed by minute data collection windows. Data at each titration point were averaged and fit to a binding isotherm using the Prism Software (Graphpad). Incubations extending longer than 5 min showed no differences in the extent of binding.

Fluorescence quenching experiments to measure binding between 5'-Fluorescein-tRNA<sup>Pro</sup> and ProRS or Hmd proteins were conducted under the same solution conditions. The fluorophore was excited at 492 nM and the emission trace monitored at protein concentrations from 0 to 4  $\mu$ M.

To measure protein-protein binding interactions, the polarization of AlexaFluor 488- labeled ProRS fluorescence was monitored as either tRNA or Hmd proteins were titrated in, using the solution conditions described above. 100 nM labeled ProRS was first introduced to the quartz micro-cuvette, mixtures were incubated for 5 minutes at room temperature at each titration point, followed by 5 minute data collection windows. In both the tRNA-protein binding and protein-protein binding assays, binding proteins were titrated in the range of 0–5  $\mu$ M final concentrations. The grating factor for the Perkin-Elmer LS55 spectrometer was determined to be 1.3 and confirmed prior to each experiment, the FL WinLab software was set to automatically correct for the grating factor in the reported polarization values.

To measure homodimer dissociation constants for *Mj*ProRS and HmdII, the fluorescence polarization of nanomolar concentrations of AlexaFluor 488-labeled protein was monitored as additional unlabeled protein was titrated in. This resulted in a binding curve that allowed calculation of the  $K_d$  representing the monomer-dimer equilibrium.

### Cell Strain and Growth

*Mj* strain JAL-1 was obtained from the Oregon Collection of Methanogens (OCM 168 = DSM 2661) and maintained in the laboratory as frozen stocks in DSM 282 medium with 25% glycerol. Cultures were routinely grown in liquid medium (DSM 282) dispensed in 25 mL aliquots into 160-mL serum bottles with a headspace of H<sub>2</sub>-CO<sub>2</sub> (80:20) pressurized to 101 kPa as described previously.<sup>49</sup> Cultures were incubated on a rotary shaker at 250 rpm at 83 °C. Growth was routinely monitored by measuring methane production and the gas phase was repressurized with H<sub>2</sub>-CO<sub>2</sub> (80:20) whenever a vacuum was detected from depletion of substrate. For preparation of cell material cultures were scaled up by sequentially inoculating six 25 mL cultures into 16 liters of selenium enriched medium in a 20 liter Bioflo IV bioreactor and 210 liters of medium in a 250 liter bioreactor (New Brunswick Scientific, Edison NJ).<sup>42</sup> Both bioreactors were maintained at 83 °C and pH 6.0 with a H<sub>2</sub>-CO<sub>2</sub> (80:20) flowrate of 0.2 vvm at  $1.7 \times 10^5$  Pa. Cells from a 250 L fermentor were harvested in late exponential growth by centrifugation in a 2 liter capacity continuous flow centrifuge (CEPA Carl Padberg Zentrifugenbau GmbH, Germany) and stored in liquid nitrogen.

### *M. jannaschii* tRNA<sup>Pro(UGG)</sup> Purification

*Mj* cell pellets weighing approximately 0.5 g (wet weight) were resuspended in 350 uL of 0.01 M sodium acetate and 0.3 M sucrose, supplemented with 100 units of RNasin (Ambion) and 40 units of RQ1 DNase (Promega), and lysed by mild sonication consisting of 5 bursts of 5 seconds at 10% duty cycle. -After incubation at 37°C for 20 minutes, a solution of 0.01 M sodium acetate and 2% SDS was added in a 1:1 ratio. The lysate was

then gently mixed by inversion and incubated at 65°C for 5 minutes. Protein and lipid fractions were then extracted by cold acid phenol:chloroform (25:1) extraction. The RNA was then recovered from the aqueous phase by ethanol precipitation.

The desired tRNA<sup>Pro</sup> isoacceptor was then isolated from total RNA via affinity purification.<sup>44</sup> tRNAs were unfolded at 50°C in the chaotropic salt tetraethylammonium chloride and allowed to hybridize to a biotinylated oligodeoxynucleotide designed to specifically bind *M. jannaschii* tRNA<sup>Pro(UGG)</sup>. The sequence of the oligodeoxynucleotide used is: 5'- CTGCCAGATTGAACGGGTCTCAGGATCCAAATCCC-BioTEG-Q-3'. Hybridization occurred during a two-step slow cooling procedure, in which the denatured RNA was cooled first to 37°C, and then to 25°C. The specifically bound tRNA was then eluted by denaturing the RNA-DNA hybrid at 65°C.

### Active Site Titration of *M. jannaschii* ProRS

The concentration of functional ProRS active sites was determined as described previously.<sup>44</sup> The initial burst of ATP consumption by the ProRS dimer was monitored as an indicator of the first catalytic turnover. Reactions were conducted in a buffer containing 50 mM HEPES (pH 7.5), 10 mM MgCl<sub>2</sub>, 100 mM NaCl, 20 mM KCl, 5 mM DTT, 5 μM ATP, 5 mM proline, 2 U/mL inorganic pyrophosphatase, and 100 cpm/μl  $\gamma$ -[<sup>32</sup>P]-ATP, the reactions were started upon the addition of 1 μM *Mj* ProRS dimer. Reaction aliquots were quenched in 400 mM sodium acetate (pH 5.2) and 0.1% SDS and separated by thin-layer chromatography (TLC) plates comprised of PEI-cellulose matrix solid phase (Sigma-Aldrich) in a mobile phase consisting of 750 mM KH<sub>2</sub>PO<sub>4</sub> (pH 3.5), 4M urea. Spots were detected by phosphorimaging and quantified with ImageQuant 5.2. ATP consumption was fit to an exponential decay curve followed by a linear phase using Kaleidagraph.

### ATP-Pyrophosphate Exchange Assay

Activation of L-proline by *Mj* ProRS was measured by pyrophosphate exchange.<sup>44</sup> Reactions were conducted in a buffer solution containing 50 mM HEPES (pH 7.5), 100 mM NaCl, 20 mM KCl, 10 mM MgCl<sub>2</sub>, 5 mM DTT, 2 mM [<sup>32</sup>P] sodium pyrophosphate, 100 nM ProRS, and 50 mM L-proline. Hmd proteins or a BSA control were included in the assay as described in Results. Aliquots were quenched in 400 mM sodium acetate (pH 5.2) and 0.1% SDS and separated on PEI-cellulose TLC plates with 750 mM KH<sub>2</sub>PO<sub>4</sub> (pH 3.5) and 4M urea as the mobile phase. Spots were detected by phosphorimaging and quantified with ImageQuant 5.2. The rate of ATP formation was fit to a linear function to obtain initial velocities. The V vs. S plots were fit to the Michaelis-Menten equation.<sup>45</sup>

### Single-Turnover Aminoacylation Assay

Under single-turnover conditions the ProRS dimer is used in molar excess over tRNA.<sup>44</sup> Radiolabeled tRNA was refolded prior to every experiment by first heating to 80°C for 3 minutes, followed by addition of MgCl<sub>2</sub> to a final concentration of 2 mM, and slow-cooling to ambient temperature over 30–45 minutes. Reactions were conducted at 37°C as described in Results. Aliquots were quenched at various time-points in a solution containing 400 mM sodium acetate (pH 5.2) and 1 unit of P1 nuclease. Quenched reactions were incubated at room temperature for 10–20 minutes to ensure complete digestion of tRNA, and subsequently spotted onto prewashed PEI-cellulose TLC plates (Sigma) and developed in a mobile phase consisting of 100 mM ammonium acetate, 5% (v/v) acetic acid. Spots corresponding to Ap\* (derived from unreacted tRNA substrate) and Pro-Ap\* (from aminoacylated product) were detected by phosphorimaging and quantified with ImageQuant 5.2. Rate constants were derived from exponential fits of product formation (Pro-tRNA<sup>Pro</sup>) with time.

## Steady-State Aminoacylation Assay

Steady-state aminoacylation assays were conducted in a buffer containing 50 mM HEPES (pH 7.5), 100 mM NaCl, 20 mM KCl, 10 mM MgCl<sub>2</sub>, and 5 mM DTT. Reactions were conducted at 37°C as described in Results. Aliquots were quenched in a solution containing 400 mM sodium acetate (pH 5.2) and 1 unit of P1 nuclease. Quenched reactions were incubated at room temperature for 10–20 minutes to ensure complete digestion of tRNA, and subsequently spotted onto prewashed PEI-cellulose TLC plates (Sigma) and developed in a mobile phase consisting of 100 mM ammonium acetate, 5% (v/v) acetic acid. Data were extracted and analyzed to determine  $k_{cat}$  and  $K_m$  as described above.

## RESULTS

### Protein Oligomerization

*Mj* Hmd, HmdII, HmdIII and ProRS were expressed in *Escherichia coli*. Each protein was independently purified via nickel affinity chromatography to 95% or better homogeneity, as assessed by SDS polyacrylamide gel electrophoresis. Quaternary structures were determined by size exclusion HPLC coupled to detection by UV absorption, static light scattering, and analysis of refractive index (Figure 1; Table 1.) All four proteins exist entirely or predominantly as dimers under conditions of moderate ionic strength (100 mM NaCl, 20 mM KCl, 10 mM MgCl<sub>2</sub>) and slightly basic pH (pH 7.5). Hmd and HmdIII also showed propensities to associate as a trimer and tetramer, respectively. These data are consistent with previous measurements on recombinant HmdII,<sup>26</sup> and with expectations for Hmd based on the crystal structure.<sup>21</sup> The finding that HmdIII is also dimeric is consistent with its high sequence similarity with HmdII. ProRS forms dimers and hexamers at a relative abundance of 2:1; the dimeric structure is consistent with prior measurements and with expectations for this class II aminoacyl-tRNA synthetase based on sequence and structural conservation with ProRS enzymes from other organisms.<sup>46</sup>

### Formation of Binary Hmd:tRNA Complexes

Preliminary data from an agarose gel shift assay suggested that HmdII binds several tRNAs.<sup>26</sup> To examine tRNA interactions in more detail, we selected five isoacceptors specific to Pro, Leu, Asp, Lys and Cys for systematic analysis with all three Hmd proteins. tRNA<sup>Asp</sup>, tRNA<sup>Lys</sup>, tRNA<sup>Leu</sup> and tRNA<sup>Pro</sup> were selected based on prior findings that the cognate tRNA synthetases form a multimeric complex *in vivo*, which may include HmdII.<sup>26–28</sup> tRNA<sup>Cys</sup> was chosen because of the unusual two-step pathway for cysteine incorporation into proteins that is unique to methanogens and closely related archaea.<sup>31</sup>

*Mj* tRNA<sup>Pro</sup> was 5'-labeled with fluorescein maleimide, and equilibrium binding to purified *Mj* ProRS and *Mj* Hmd proteins was measured by fluorescence anisotropy using low concentrations of tRNA and titrating with increasing quantities of protein.  $K_d$  for binding to ProRS was determined to be 1.5  $\mu$ M, equivalent to prior measurements by electrophoretic mobility shift assay.<sup>46</sup> By this approach we then found that both HmdII and HmdIII also form binary complexes with tRNA<sup>Pro</sup> with nearly identical affinities in the 1–2  $\mu$ M range (Table 2; Figure 2). However, while binding to Hmd could be detected, no saturation was observed at protein concentrations up to 25  $\mu$ M. Thus, only the paralogs bind tRNA<sup>Pro</sup> with affinities in a range that is comparable to ProRS and that is therefore likely to be physiologically relevant.

We then extended these measurements to the other tRNAs using an electrophoretic mobility shift assay (EMSA) with low concentrations of 3'-<sup>32</sup>P labeled tRNA, which facilitated much more rapid data collection. For all four other tRNAs examined, we consistently found very weak binding to Hmd and, with the partial exception of tRNA<sup>Lys</sup>, tighter binding to HmdII

with affinities similar to those measured by fluorescence (Table 2; Figure 3). Binding to HmdIII was detected at an intermediate level, although for tRNA<sup>Pro</sup> this interaction appears significantly weaker when measured by EMSA as compared with fluorescence. Neither HmdII nor HmdIII exhibited strong preference for particular tRNAs. No gel shift was observed in control experiments in which tRNAs were preincubated with bovine serum albumin (BSA).

Together, these data suggest that HmdII binds tRNA molecules with physiologically relevant affinity ( $\mu\text{M}$  range) but with little specificity, consistent with prior work.<sup>26</sup> The interactions of HmdIII with tRNA<sup>Pro</sup> are also in this range. However, Hmd binds tRNA much more weakly. The consistency of this finding for a variety of tRNAs provides support for the general notion that the paralog Hmd proteins, but not Hmd, exhibit tRNA binding properties. However, interactions of HmdII and HmdIII with tRNA<sup>Pro</sup> were not detected by SEC-MALS under conditions in which the ProRS-tRNA<sup>Pro</sup> complex was readily isolated (Supplementary Figure 1), despite the nearly identical affinities. Possibly, the HmdII and HmdIII complexes with tRNA may exhibit faster association and dissociation kinetics, so that stable complexes could not be maintained over the relatively long timescale required for HPLC separation (~20 minutes). For the ProRS-tRNA<sup>Pro</sup> interaction, analysis of  $A_{260}/A_{280}$  ratios and the refractive index gradient, for both isolated components and the complex, indicated a binding stoichiometry of one tRNA molecule per dimer (see Methods). This data is consistent with the demonstration of half-of-the-sites activity for this enzyme.<sup>44</sup>

### Formation of Protein-Protein Complexes

Fluorescence polarization was also used to examine binary interactions between ProRS and each Hmd protein. For these experiments ProRS was labeled with Alexa-Fluor 488-TFPE at a 1:6 stoichiometric ratio with protein dimer. Using the single-turnover assay, we confirmed that tRNA binding and protein activity were not compromised upon labeling (data not shown). As a further control, the  $K_d$  of Alexafluor-labeled ProRS for tRNA<sup>Pro</sup> was measured at 2.4  $\mu\text{M}$ , which is nearly identical to the value determined for this interaction using radiolabeled tRNA<sup>Pro</sup> (Figure 4; Table 2). A negative control using BSA produced a much smaller amplitude; the small signal registered may arise from molecular crowding and a consequent alteration in the environment of the fluorophore. The decrease in polarization upon tRNA binding appears surprising, but this phenomenon has been observed previously, and may arise from displacement of the nonpolar fluorophore from the ProRS surface upon tRNA binding, giving rise to greater rotational mobility about the connecting linker.<sup>39,47</sup> Each Hmd protein was then titrated into the labeled ProRS and the equilibrium fluorescence polarization recorded. Interestingly, ProRS binds all three Hmd proteins in the 1–2  $\mu\text{M}$  range (Figure 4).<sup>26</sup> Thus, unlike the specific tRNA<sup>Pro</sup> binding only to HmdII and HmdIII, the interaction of ProRS is nonspecific with respect to the identity of the Hmd protein (Table 3). An analogous experiment performed with the Alexafluor label located on HmdII further confirms binary protein-protein complex formation in this case (Supplementary Figure S2).

### Ternary Complex Formation

Both EMSA and fluorescence polarization were employed to examine ternary complex formation. Addition of Hmd to the preformed ProRS-tRNA<sup>Pro</sup> complex produced a linear increase in fluorescence polarization, but no saturation was observed at concentrations up to 15  $\mu\text{M}$  Hmd (Figure 5A). Further, Hmd did not produce a supershift of the ProRS-tRNA<sup>Pro</sup> complex on native acrylamide gels (Figure 5B). In contrast, specific ternary complex formation was observed for HmdII and HmdIII by both approaches. Using 5'-fluorescein labeled tRNA at concentrations of approximately 5 nM, we first recorded ProRS binding to a saturating level in the micromolar range (Figures 5C, 5D). Next, HmdII or HmdIII were titrated into the reaction mixture. For both homologs, the polarization increases further,

reaching a new saturation level after addition to the micromolar concentration range. The further decrease in rotational mobility upon HmdII or HmdIII binding to the binary complex offers strong evidence of ternary complex formation. Performing the protein titrations in reverse order confirms ternary complex formation in the same concentration range (Supplementary Figure S3). EMSA experiments also demonstrated that titration of HmdII or HmdIII into solutions containing the preformed ProRS-tRNA<sup>Pro</sup> complex produced a supershift in both cases (Figure 5E). To assign the identities of the supershifted proteins, the relevant supershifted bands were excised and their contents analyzed by SDS-PAGE (Figure 5F). Densitometry performed on the protein bands separated in lane A (Figure 5F) suggest that HmdII and ProRS are present in a 1:1 stoichiometric ratio in the ternary complex. Together, these experiments offer strong evidence for the formation of ternary ProRS-tRNA<sup>Pro</sup>-Hmd complexes with the HmdII and HmdIII paralogs.

To assess whether HmdII and ProRS bind tRNA in similar orientations, we monitored fluorescence intensity changes of 5'-fluorescein-tRNA<sup>Pro</sup> upon protein binding. While fluorescence quenching was observed upon ProRS binding, no fluorescence intensity change was observed upon HmdII binding to tRNA at 5–10 μM concentrations (Figure 6). The failure to observe fluorescence quenching from the site-specific 5'-tRNA probe, under saturating conditions where binding is known to occur as monitored by both EMSA and fluorescence anisotropy (Figures 2, 3), suggests that HmdII does not interact with tRNA in the vicinity of its 5'-end. In contrast, the strong quenching signal indicates that, in contrast, ProRS does bind at the tRNA 5'-end.

### Effects of Hmd Protein Binding on ProRS Kinetics

To determine whether Hmd binding modulates ProRS function, we characterized the kinetics of prolyl adenylate and Pro-tRNA<sup>Pro</sup> formation by a variety of approaches. We first titrated the active sites by measuring depletion of  $\gamma^{32}\text{P}$ -ATP, via the ProRS-catalyzed reaction of the ATP with proline to form prolyl adenylate and pyrophosphate (first step of the two-step aminoacylation reaction) (Supplementary Figure 4). The initial burst corresponds to the first enzyme turnover, so that extrapolation to the ordinate permits determination of the number of active sites. The value determined is 0.7 active sites per dimer, consistent with the notion of half-of-the-sites activity for the dimer.<sup>46</sup> Inclusion of each Hmd protein at 5 μM concentration, in molar excess to ProRS, did not affect the observed kinetics of this reaction or the calculated proportion of enzyme that is catalytically active (Supplementary Figure 4).

We next monitored L-proline activation by ATP-PP<sub>i</sub> exchange, which measures the approach to equilibrium for the reverse reaction whereby the radiolabel initially present in the pyrophosphate is incorporated into ATP. The presence of Hmd proteins at 5 μM concentration decreases the maximum velocity of the reaction at saturating proline levels by approximately two-fold, with compensating effects on  $K_m$  for proline (Table 4). This suggests that binding of these proteins has the capacity to exert a regulatory effect on ProRS activity in the cell. Effects of similar magnitude on tRNA synthetase activities were observed upon multisynthetase complex formation by *Mt* enzymes.<sup>27,28</sup>

The effect of Hmd proteins on the ProRS-catalyzed formation of Pro-tRNA<sup>Pro</sup> under both single-turnover and steady-state conditions was also studied. Because unmodified transcripts of tRNA produced by *in vitro* transcription were poorly aminoacylated, we isolated post-transcriptionally modified, homogeneous tRNA<sup>Pro</sup> by affinity purification from *M. jannaschii* cells without overproduction. This native tRNA preparation performed substantially better in all assays, exhibiting plateau aminoacylation levels of approximately 50% in single-turnover assays at 5 μM ProRS dimer, 50 nM tRNA, and saturating levels of proline and ATP (50 mM and 5 mM, respectively) (Supplementary Figure S5). Inclusion of

any of the three Hmd proteins at 5 uM concentration decreases plateau aminoacylation by about 10% under single-turnover conditions, but little difference was observed in the rate of product formation. Performing the tRNA refolding reaction in the presence of any of the Hmd proteins did not alter the plateau levels or rate of aminoacylation, suggesting that the proteins do not function as folding chaperones. Under steady-state conditions containing 15 nM ProRS dimer, 150 nM tRNA<sup>Pro</sup>, 100 mM L-proline and 10 mM ATP, we also did not observe a significant effect on the rate of product formation upon inclusion of any of the three Hmd proteins at 5 μM concentration. It appears then that the influence of Hmd proteins on ProRS kinetics is limited to quantitatively small effects at the activation step of the reaction.

## DISCUSSION

Several lines of experimental evidence now support the notion that the functional roles of the HmdII and HmdIII paralogs are distinct from that of Hmd. First, it was demonstrated previously that purified HmdII and HmdIII proteins obtained via heterologous expression in *E. coli* do not possess the H<sub>2</sub>-dependent dehydrogenase activity of Hmd, nor are they active as hydrogenases using a variety of other electron acceptors.<sup>7</sup> Nonetheless, the earlier findings that HmdII can compete with Hmd for cofactor binding in *in vitro* experiments,<sup>20</sup> and that the three Hmd proteins in *Mt* are differentially regulated in response to nickel and H<sub>2</sub> concentrations *in vivo*,<sup>7</sup> suggests that both paralogs retain some importance for hydrogenotrophic methanogenesis. Since a direct role in the chemistry of substrate processing appears unlikely, it may be valuable to consider whether the paralogs could instead be involved in modulating the flux through the methanogenesis pathway, and thus in turn the energy charge of the cell, in response to environmental stimuli.

The other experimental basis for considering a distinct function for HmdII and HmdIII originates with the earlier finding that HmdII copurifies with ProRS from native *Mj* cell lysates.<sup>25,26</sup> This is of interest because it suggests the possibility of a metabolic linkage between methanogenesis and protein synthesis. We have now extended this work to examine the interactions of all three Hmd proteins with components of the protein synthesis machinery. The most important new insight from our experiments is that the binary complexes formed with tRNA, and the ternary complexes formed with tRNAPro and ProRS, are specific only to the HmdII and HmdIII paralog proteins (Figures 2, 3, 5). In contrast, the Hmd enzyme that directly participates in methanogenesis does not bind tRNA in a concentration range that is likely to be physiologically significant, nor does it form a stable ternary complex with tRNA and aminoacyl-tRNA synthetase. This provides a clear functional separation that presumably has its origins in differences among the tertiary structures of the Hmd proteins. Significantly, the shared functional roles of HmdII and HmdIII in binding tRNA and aminoacyl-tRNA synthetase are reflected in their 80% shared identity at the primary sequence level. Conversely, HmdII and HmdIII share only 20% identity with Hmd, although the level of similarity is sufficient to infer that the overall folding topologies of at least the central active site-containing domain are the same.<sup>20,24</sup> Considering the sequence alignment in light of the known structure of Hmd then suggests that significant structural differences occur throughout both the larger N-terminal domain that contains the Hmd catalytic site, and are particularly pronounced in the C-terminal dimer interface region (Figure 7).<sup>24</sup> Further, a 30 amino acid C-terminal extension that is rich in highly conserved basic amino acids is unique to the paralogs;<sup>20</sup> we speculate that this peptide may function as an RNA binding determinant. These structure-based sequence analyses provide the basis for mutational studies to address which amino acids are responsible for the unique binding activities of HmdII and HmdIII.

The architecture of the ternary complexes formed by HmdII or HmdIII with ProRS and tRNA<sup>Pro</sup> is not yet established. However, the 1:1 stoichiometry of HmdII with ProRS deduced from the gel shift experiments (Figure 5), together with the finding from SEC-MALS that the ProRS dimer binds one tRNA, suggests that the complex may minimally consist of a single tRNA bound to dimers of ProRS and HmdII. Since all three Hmd proteins form binary complexes with ProRS, while only HmdII and HmdIII form binary complexes with tRNA at concentrations likely to be physiologically relevant, it appears that the interactions of tRNA with the paralogs must be essential to ternary complex stability. One possible model is that unique amino acid determinants present only in HmdII and HmdIII might allow simultaneous ProRS and tRNA<sup>Pro</sup> binding by these proteins, while the absence of such residues could prevent Hmd from associating with a ProRS-tRNA<sup>Pro</sup> complex. The crystal structure of an archaeal class ProRS with tRNA is only available as a (possibly) early-stage docking complex with just the anticodon loop bound to the enzyme,<sup>48</sup> but in general, a substantial unbound surface of the tRNA remains accessible to ternary complex formation in all known aminoacyl-tRNA synthetase:tRNA complexes.

Mechanisms for metabolic regulation in methanogens have mainly been described at the transcriptional level.<sup>6</sup> However, the relatively long time periods required for RNA and protein biosynthesis in response to changing environmental cues suggest the desirability of a more rapid response that could be highly adaptive given the usual conditions of energetic stress in which the organisms operate. In this context, the novel HmdII/HmdIII interactions with components of the protein synthesis machinery may be of particular relevance when ambient H<sub>2</sub> concentrations are particularly low and both *hmdII* and *hmdIII* genes are more highly expressed.<sup>8</sup> Under these conditions in which a decreased rate of ATP synthesis is also likely, sequestration of tRNA and aminoacyl-tRNA synthetase by Hmd paralogs could conserve metabolic energy by slowing the rate of protein synthesis. This notion should be testable in *in vivo* experiments. Another possibility is that tRNA and aminoacyl-tRNA synthetase binding may influence the capacity of the Hmd paralogs to bind/sequester the FeGP cofactor *in vivo* or perhaps to facilitate its transfer to active Hmd.<sup>20,24</sup> Thus, the interactions between Hmd paralogs and tRNA may provide an example in which complex formation between components of two distinct pathways may influence the function of both.

## Supplementary Material

Refer to Web version on PubMed Central for supplementary material.

## Acknowledgments

This research was supported by NIH grant GM63713 (to J.J.P.) and the Department of Energy, Biological and Environmental Research, Grant No. DE-FG02-07ER64502 to K.R.S.

## ABBREVIATIONS

<b>aaRS</b>	aminoacyl-tRNA synthetases
<b>EMSA</b>	electrophoretic mobility shift assay
<b>SEC-MALS</b>	size exclusion chromatography coupled to multiangle light scattering
<b>H<sub>4</sub>MPT</b>	tetrahydromethanopterin
<b>TBE</b>	Tris-Borate-EDTA
<b>BSA</b>	bovine serum albumin
<b>TLC</b>	thin-layer chromatography

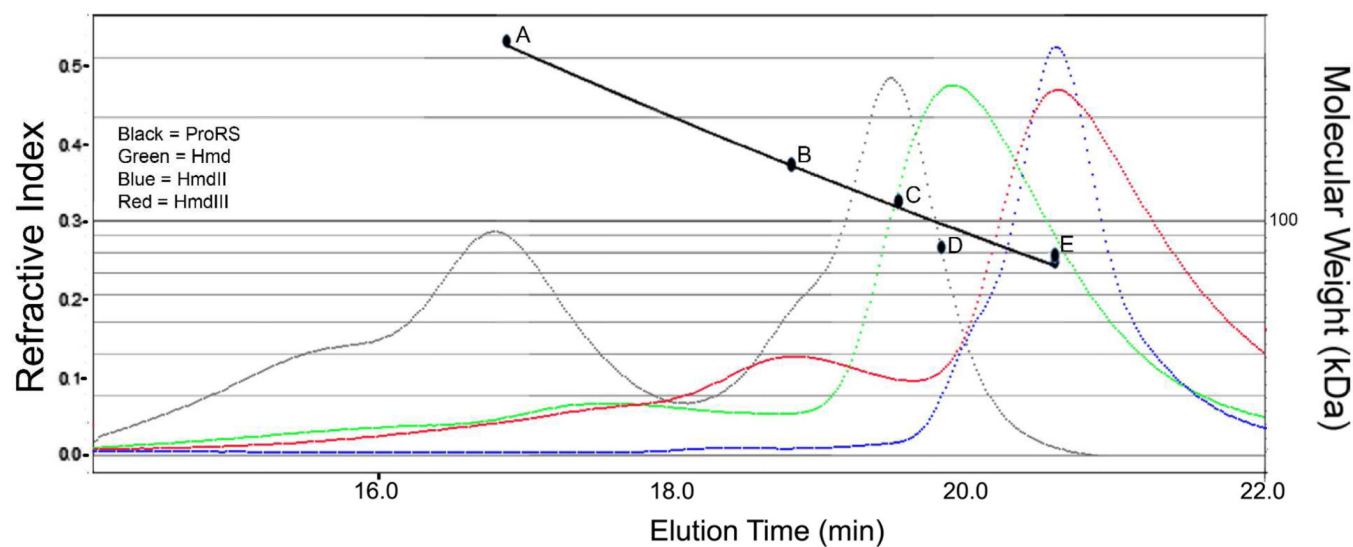
<b>SDS</b>	sodium dodecyl sulfate
<b>Mj</b>	<i>Methanocaldococcus jannaschii JAL-1</i>
<b>Mt</b>	<i>Methanothermobacter thermoautotrophicus ΔH</i>

## REFERENCES

1. Deppenmeier U. The unique biochemistry of methanogenesis. *Prog. Nucleic Acid Mol. Biol.* 2002; 71:222–283.
2. Thauer RK, Kaster A-K, Seedorf H, Buckel W, Hedderich R. Methanogenic archaea: ecologically relevant differences in energy conservation. *Nat. Rev. Microbiol.* 2008; 6:579–591. [PubMed: 18587410]
3. Deppenmeier U, Müller V. Life close to the thermodynamic limit: how methanogenic archaea conserve energy. *Results Probl Cell Differ.* 2008; 45:123–152. [PubMed: 17713742]
4. Muller, V.; Blaut, M.; Gottschalk, G. Bioenergetics of methanogenesis. In: Ferry, JG., editor. *Methanogenesis*. New York & London: Chapman and Hall; 1993. p. 360–406.
5. Valentine DL. Adaptations to energy stress dictate the ecology and evolution of the Archaea. *Nat. Rev. Microbiol.* 2007; 5:316–323. [PubMed: 17334387]
6. Morgan RM, Pihl TD, Nölling J, Reeve JN. Hydrogen regulation of growth, growth yields, and methane gene transcription in *Methanobacterium thermoautotrophicum ΔH*. *J. Bacteriol.* 1997; 179:889–898. [PubMed: 9006047]
7. Afting C, Kremmer E, Brucker C, Hochheimer A, Thauer RK. Regulation of the synthesis of H<sub>2</sub>-forming methylenetetrahydromopterin dehydrogenase (Hmd) and of HmdII and HmdIII in *Methanothermobacter marburgensis*. *Arch. Microbiol.* 2000; 174:225–232. [PubMed: 11081790]
8. Reeve JN, Nölling J, Morgan RM, Smith DR. Methanogenesis: genes, genomes, and who's on first? *J Bacteriol.* 1997; 179:5975–5986. [PubMed: 9324240]
9. Hendrickson EL, Haydock AK, Moore BC, Whitman WB, Leigh JA. Functionally distinct genes regulated by hydrogen limitation and growth rate in methanogenic Archaea. *Proc. Natl. Acad. Sci. USA.* 2007; 104:8930–8934. [PubMed: 17502615]
10. Keltjens JT, Vogels GD. Metabolic regulation in methanogenic Archaea during growth on hydrogen and CO<sub>2</sub>. *Environmental Monitoring and Assessment.* 1996; 42(1–2):19–37.
11. Schworer B, Thauer RK. Activities of formylmethanofuran dehydrogenase, methylenetetrahydromopterin dehydrogenase, methylenetetrahydromopterin reductase, and heterodisulfide reductase in methanogenic bacteria. *Arch. Microbiol.* 1991; 155:459–465.
12. von Bunau R, Zirngibl C, Thauer RK, Klein A. Hydrogen-forming and coenzyme-F<sub>420</sub>-reducing methylene tetrahydromopterin dehydrogenases are genetically distinct enzymes in *Methanobacterium thermoautotrophicum* (Marburg). *Eur. J. Biochem.* 1991; 202:1205–1208. [PubMed: 1765081]
13. Mukhopadhyay B, Purwantini E, Pihl TD, Reeve JN, Daniels L. Cloning, sequencing, and transcriptional analysis of the coenzyme F<sub>420</sub>-dependent methylene-5,6,7,8-tetrahydromopterin dehydrogenase gene from *Methanobacterium thermoautotrophicum* strain Marburg and functional expression in *Escherichia coli*. *J. Biol. Chem.* 1995; 270:2827–2832. [PubMed: 7852356]
14. Vaupel M, Thauer RK. Two F<sub>420</sub>-reducing hydrogenases in *Methanosaarcina barkeri*. *Arch. Microbiol.* 1998; 169:201–205. [PubMed: 9477253]
15. Zirngibl C, Hedderich R, Thauer RK. N<sub>5</sub>,N<sub>10</sub>-methylene tetrahydromopterin dehydrogenase from *Methanobacterium thermoautotrophicum* has hydrogenase activity. *FEBS Lett.* 1990; 261:112–116.
16. Afting C, Hochheimer A, Thauer RK. Function of H<sub>2</sub>-forming methylenetetrahydromopterin dehydrogenase from *Methanobacterium thermoautotrophicum* in coenzyme F<sub>420</sub> reduction with H<sub>2</sub>. *Arch. Microbiol.* 1998; 169:206–210. [PubMed: 9477254]
17. Hendrickson EL, Leigh JA. Roles of coenzyme F<sub>420</sub>-reducing hydrogenases and hydrogen- and F<sub>420</sub>-dependent methylenetetrahydromopterin dehydrogenases in reduction of F<sub>420</sub> and

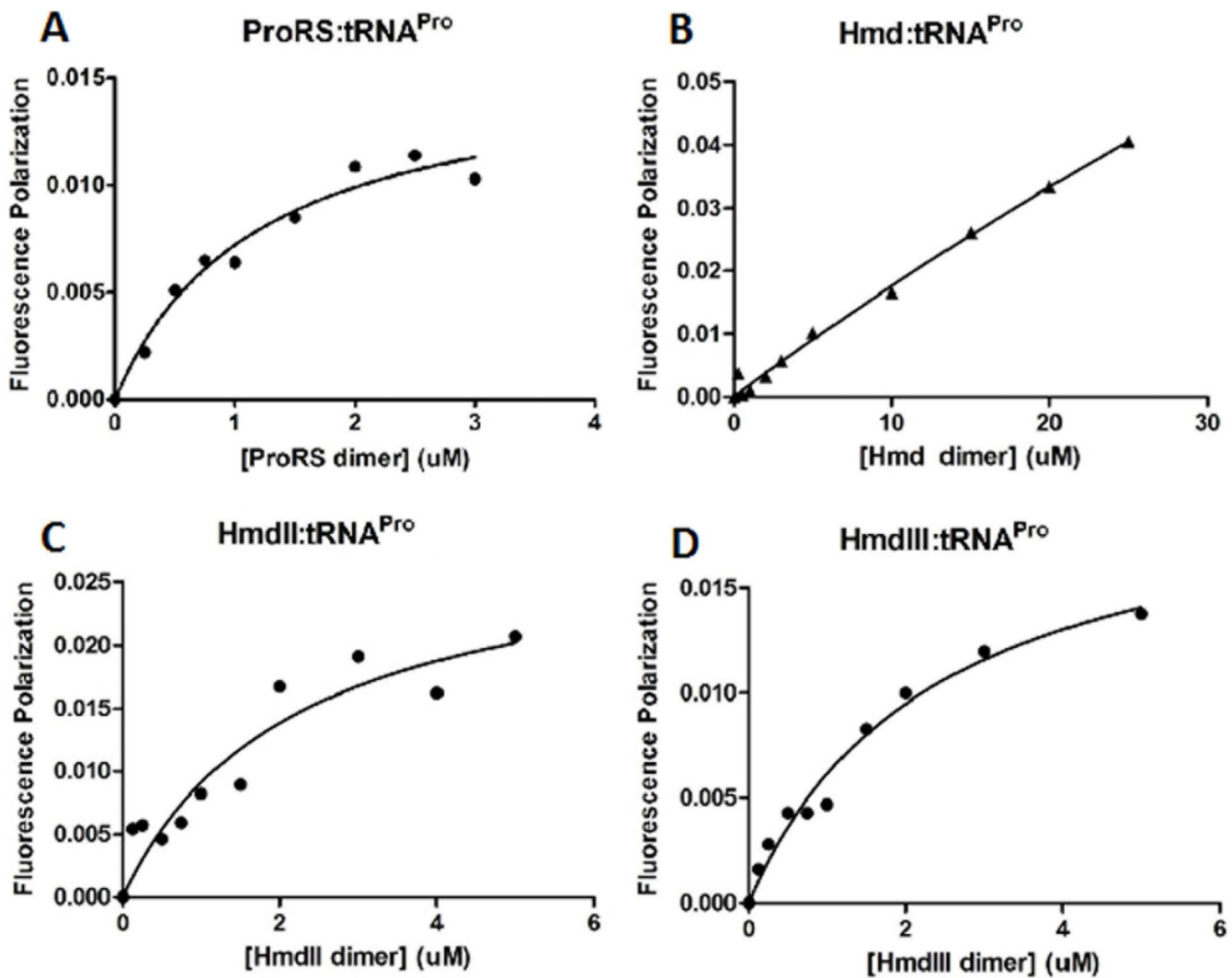
- production of hydrogen during methanogenesis. *J. Bacteriol.* 2008; 190:4818–4821. [PubMed: 18487331]
18. Shima S, Pilak O, Vogt S, Schick M, Stagni MS, Meyer-Klaucke W, Warkentin E, Thauer RK, Ermler U. The crystal structure of [Fe]-hydrogenase reveals the geometry of the active site. *Science*. 2008; 321:572–575. [PubMed: 18653896]
  19. Korbas M, Vogt S, Meyer-Klaucke W, Bill E, Lyon EJ, Thauer RK. The iron-sulfur cluster-free hydrogenase (Hmd) is a metalloenzyme with a novel iron binding motif. *J. Biol. Chem.* 2006; 281:30804–30813. [PubMed: 16887798]
  20. Shima S, Thauer RK. A third type of hydrogenase catalyzing H<sub>2</sub> activation. *The Chemical Record*. 2007; 7:37–46.
  21. Pilak O, Mamat B, Vogt S, Hagemeier CH, Thauer RK, Shima S, Vonrhein C, Warkentin E, Ermler U. The crystal structure of the apoenzyme of the iron-sulphur cluster-free hydrogenase. *J. Mol. Biol.* 2006; 358:798–809. [PubMed: 16540118]
  22. Smith DR, Doucette-Stamm LA, Deloughery C, Lee H, Dubois J, Aldredge T, et al. Complete genome sequence of *Methanobacterium thermoautotrophicum* ΔH: functional analysis and comparative genomics. *J. Bacteriol.* 1997; 179:7135–7155. [PubMed: 9371463]
  23. Bult CJ, White O, Olsen GJ, Zhou L, Fleischmann RD, Sutton GG, Blake JA, et al. Complete genome sequence of the methanogenic archaeon *Methanococcus janaschii*. *Science*. 1996; 273:1058–1073. [PubMed: 8688087]
  24. Goldman AD, Leigh JA, Samudrala R. Comprehensive computational analysis of Hmd enzymes and paralogs in methanogenic Archaea. *BMC Evolutionary Biology*. 2009; 9:199. [PubMed: 19671178]
  25. Lipman RS, Sowers KR, Hou YM. Synthesis of cysteinyl-tRNA(Cys) by a genome that lacks the normal cysteine-tRNA synthetase. *Biochemistry*. 2000; 39:7792–7798. [PubMed: 10869184]
  26. Lipman RSA, Chen J, Evilia C, Vitseva O, Hou Y-M. Association of an aminoacyl-tRNA synthetase with a putative metabolic protein in archaea. *Biochemistry*. 2003; 42:7487–7496. [PubMed: 12809505]
  27. Hausmann CD, Ibba M. Structural and functional mapping of the archaeal multi-aminoacyl-tRNA synthetase complex. *FEBS Lett.* 2008; 582:2178–2182. [PubMed: 18538672]
  28. Praetorius-Ibba M, Hausmann CD, Paras M, Rogers TE, Ibba M. An aminoacyl-tRNA synthetase:elongation factor complex for substrate channeling in archaeal translation. *Nucl. Acids Res.* 2007; 35:6094–6102. [PubMed: 17766929]
  29. Guo M, Yang X-L, Schimmel P. New functions of aminoacyl-tRNA synthetases beyond translation. *Nat. Rev. Mol. Cell Biol.* 2010; 11:668–674. [PubMed: 20700144]
  30. Potrykus K, Cashel M. (p)ppGpp: still magical? *Annu. Rev. Microbiol.* 2008; 62:35–51. [PubMed: 18454629]
  31. Sauerwald A, Zhu W, Major TA, Roy H, Palioura S, Jahn D, Whitman WB, Yates JR 3d, Ibba M, Soll D. RNA-dependent cysteine biosynthesis in archaea. *Science*. 2005; 307:1969–1972. [PubMed: 15790858]
  32. Blight SK, Larue RC, Mahapatra A, Longstaff DG, Chang E, Zhao G, Kang PT, Green-Church KB, Chan MK, Krzycki JA. Direct charging of tRNA(CUA) with pyrrolysine *in vitro* and *in vivo*. *Nature*. 2004; 431:333–335. [PubMed: 15329732]
  33. Sherlin LD, Bullock TL, Nissan TA, Perona JJ, Lariviere FJ, Uhlenbeck OC, Scaringe SA. Chemical and enzymatic synthesis of tRNAs for high-throughput crystallization. *RNA*. 2001; 7:1671–1678. [PubMed: 11720294]
  34. Kawamura T, Vartanian AS, Zhou H, Dahlquist FW. The design involved in PapI and Lrp regulation of the *pap* operon. *J. Mol Biol.* 2011; 409:311–332. [PubMed: 21338611]
  35. Glasel JA. Validity of nucleic acid purities monitored by 260nm/280nm absorbance ratios. *BioTechniques*. 1995; 18:62–63. [PubMed: 7702855]
  36. Di Primo C, Lebars I. Determination of refractive index increment ratios for protein-nucleic acid complexes by surface plasmon resonance. *Anal. Biochem.* 2007; 368:148–155. [PubMed: 17659251]

- NIH-PA Author Manuscript NIH-PA Author Manuscript NIH-PA Author Manuscript
37. Rodríguez-Hernández A, Bhaskaran H, Hadd A, Perona JJ. Synthesis of Glu-tRNA(Gln) by engineered and natural aminoacyl-tRNA synthetases. *Biochemistry*. 2010; 49:6727–6736. [PubMed: 20617848]
  38. Buratowski, S.; Chodosh, LA. Mobility shift DNA-binding assay using gel electrophoresis. In: Ausubel, Frederick M., editor. *Current protocols in molecular biology*. Vol. Chapter 12. 2001. Unit 12.2
  39. Jameson DM, Sawyer WH. Fluorescence anisotropy applied to biomolecular interactions. *Meth. Enzymol.* 1995; 246:283–300. [PubMed: 7752928]
  40. Chan B, Weidemaier K, Yip WT, Barbara PF, Musier-Forsyth K. Intra-tRNA distance measurements for nucleocapsid protein-dependent tRNA unwinding during priming of HIV reverse transcription. *Proc. Natl. Acad. Sci. USA*. 1999; 96:459–464. [PubMed: 9892655]
  41. Sowers, KR.; Watts, JEM. Methods for the study of strictly anaerobic microorganisms. In: Oren, FARaA, editor. *Methods in Microbiology – Extremophiles*. Vol. vol. 35. Oxford: Elsevier/Academic Press; 2006.
  42. Mukhopadhyay B, Johnson EF, Wolfe RS. Reactor-scale cultivation of the hyperthermophilic methanarchaeon *Methanococcus jannaschii* to high cell densities. *Appl. Environ. Microbiol.* 1999; 65:5059–5065. [PubMed: 10543823]
  43. Yokogawa T, Kitamura Y, Nakamura D, Ohno S, Nishikawa K. Optimization of the hybridization-based method for purification of thermostable tRNAs in the presence of tetraalkylammonium salts. *Nucleic Acids Res.* 2010; 38:e89. [PubMed: 20040572]
  44. Francklyn CS, First EA, Perona JJ, Hou Y-M. Methods for kinetic and thermodynamic analysis of aminoacyl-tRNA synthetases. *Methods*. 2008; 44:100–118. [PubMed: 18241792]
  45. Fersht, AR. *Structure and Mechanism in Protein Science*. New York: W.H. Freeman and Company; 1999. p. 296-304.
  46. Ambrogelly A, Kamtekar S, Stathopoulos C, Kennedy D, Söll D. Asymmetric behavior of archaeal prolyl-tRNA synthetase. *FEBS Lett.* 2005; 57:6017–6022. [PubMed: 16226256]
  47. Lakowicz, JR. *Principles of Fluorescence Spectroscopy*. 2nd ed.. New York: Kluwer Academic / Plenum Publishers; 1999. p. 291-319.
  48. Yaremcuk A, Cusack S, Tukalo M. Crystal structure of a eukaryote/archaeon-like prolyl-tRNA synthetase and its complex with tRNA<sup>Pro</sup>. *EMBO J.* 2000; 19:4745–4758. [PubMed: 10970866]
  49. Menezes S, Kirk G, Krivos KL, Apolinario EE, Reich NO, Sowers K, Limbach P, Perona JJ. Enzymatic synthesis of tRNA m<sup>2</sup>G6 in thermophilic methanogens by the novel tRNA methyltransferase Trm14. *Nucleic Acids Res.* 2011; 39:7641–7655. [PubMed: 21693558]

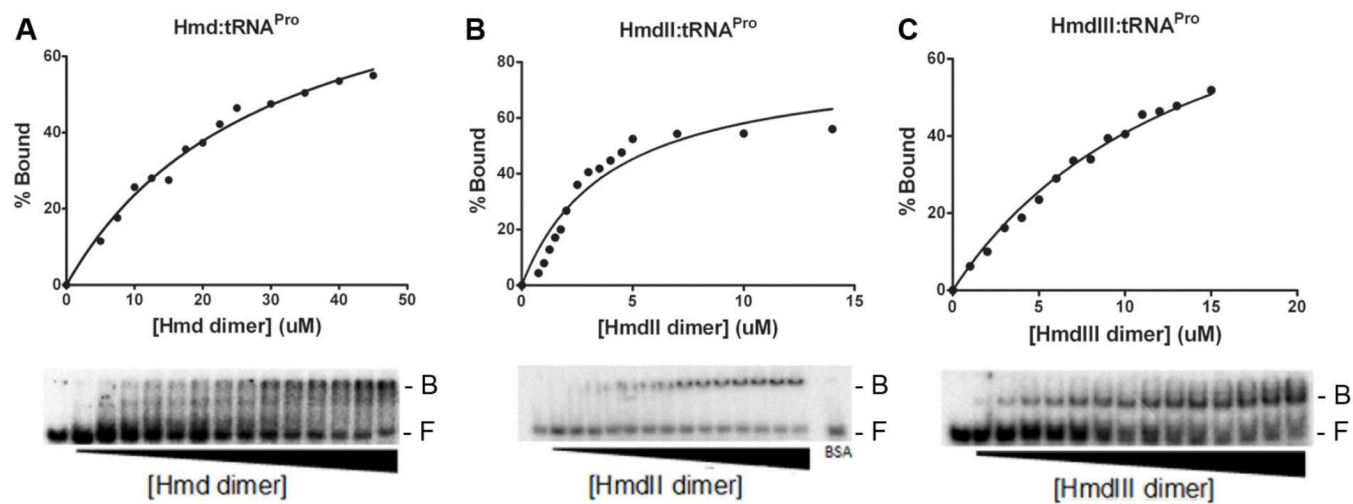


**Figure 1.**

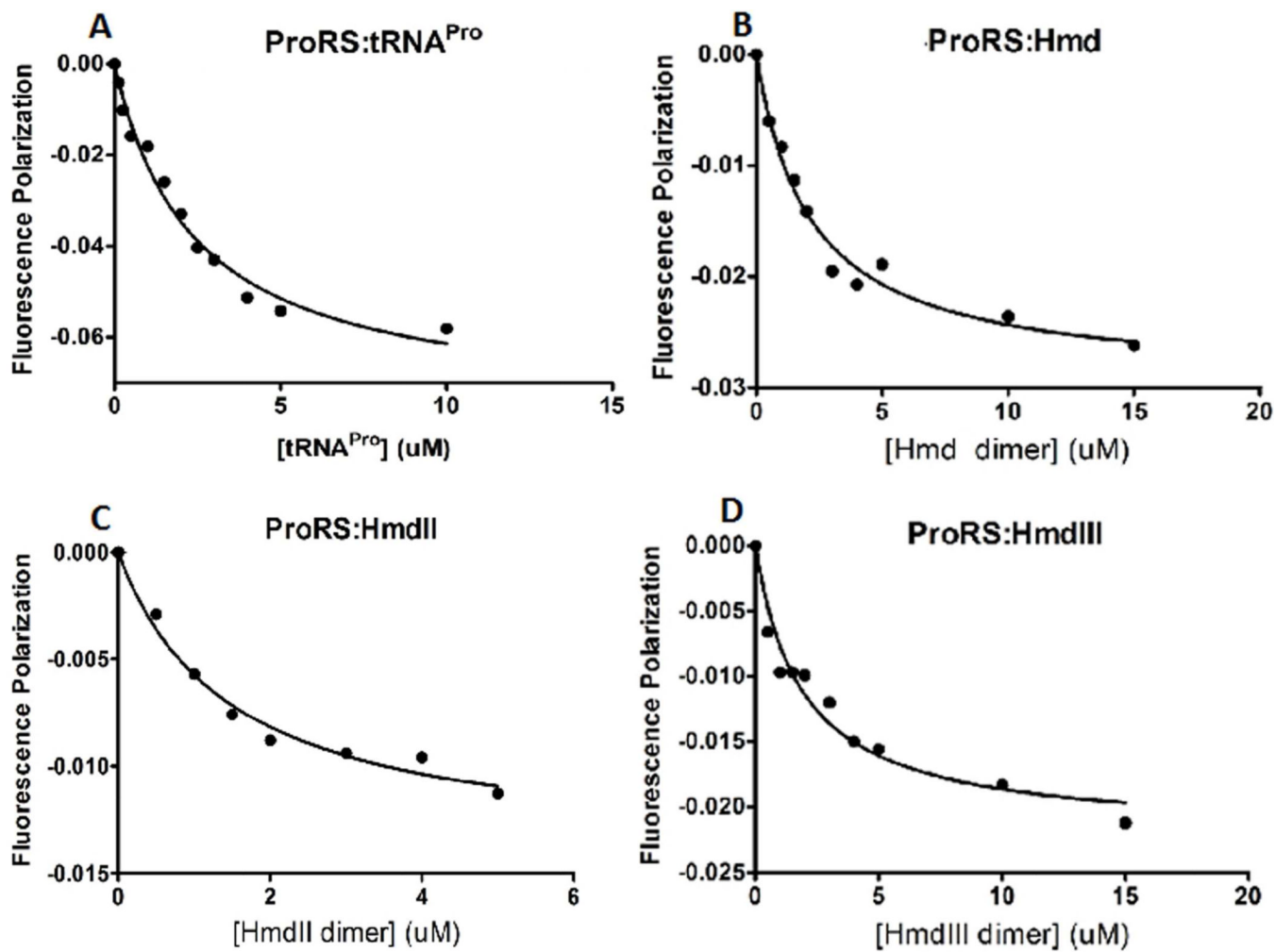
Size exclusion HPLC coupled to multiangle light scattering. Superimposed runs for ProRS, Hmd and Hmd paralogs are shown color-coded as indicated. The plot depicts the logarithm of the molecular weight on the ordinate and the elution time on the abscissa. The second ordinate depicts the refractive index gradient. Molecular weights were determined from the light scattering data.

**Figure 2.**

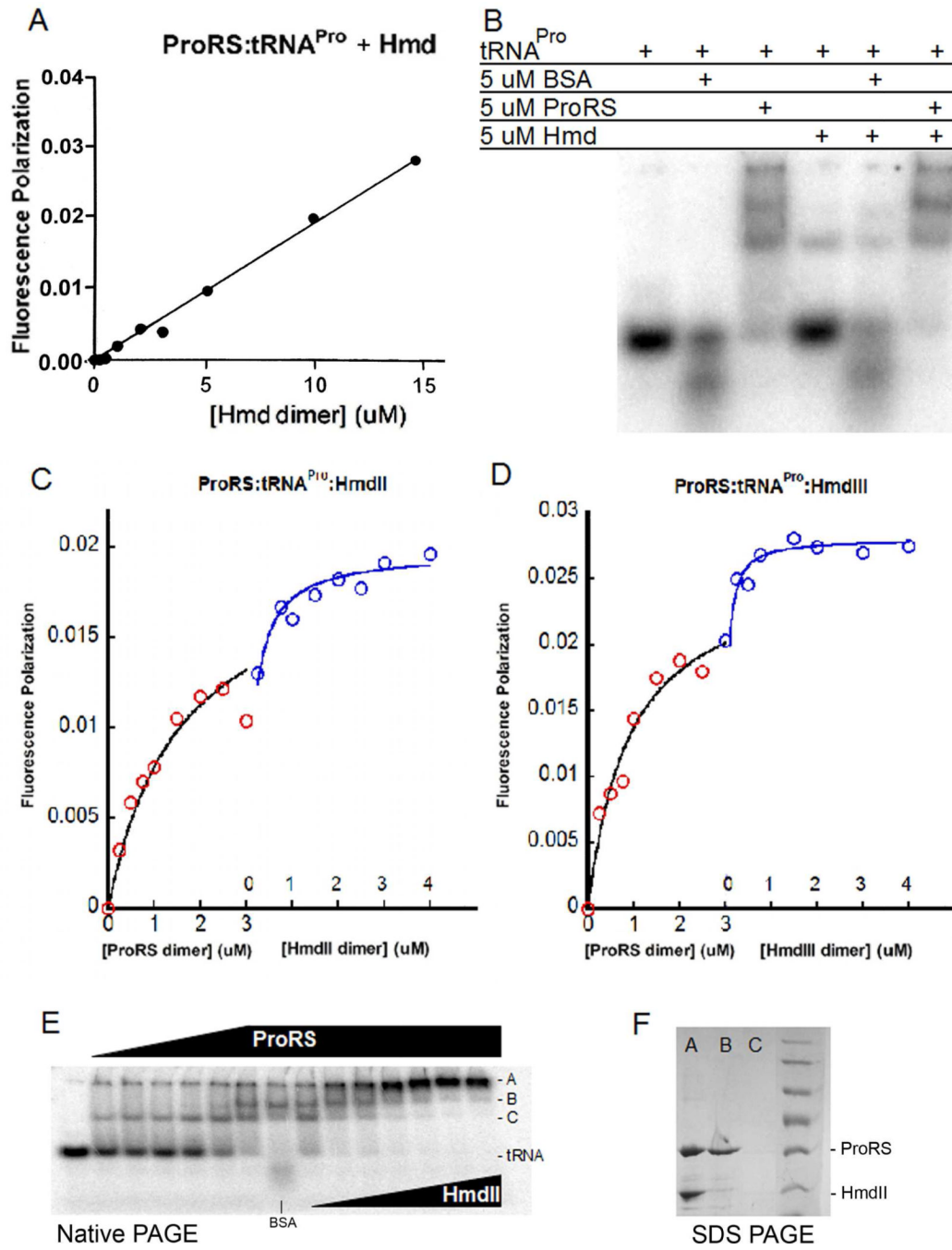
Formation of Hmd-tRNA<sup>Pro</sup> binary complexes measured by steady-state fluorescence anisotropy for Hmd (panel B), HmdII (panel C) and HmdIII (panel D). The fluorescent label is present as 5'-fluorescein conjugated tRNA<sup>Pro</sup>. The control experiment using the identical methodology to measure the affinity of the ProRS-tRNA<sup>Pro</sup> complex is shown in panel A.

**Figure 3.**

EMSA depicting binary complex formation between Hmd proteins and tRNA<sup>Pro</sup>. Native PAGE show the mobility shift of 3'-labeled tRNA upon binding as Hmd (A), HmdII (B), or HmdIII (C) are titrated in. The fraction of bound tRNA is shown as a function of the dimeric concentration of each protein.

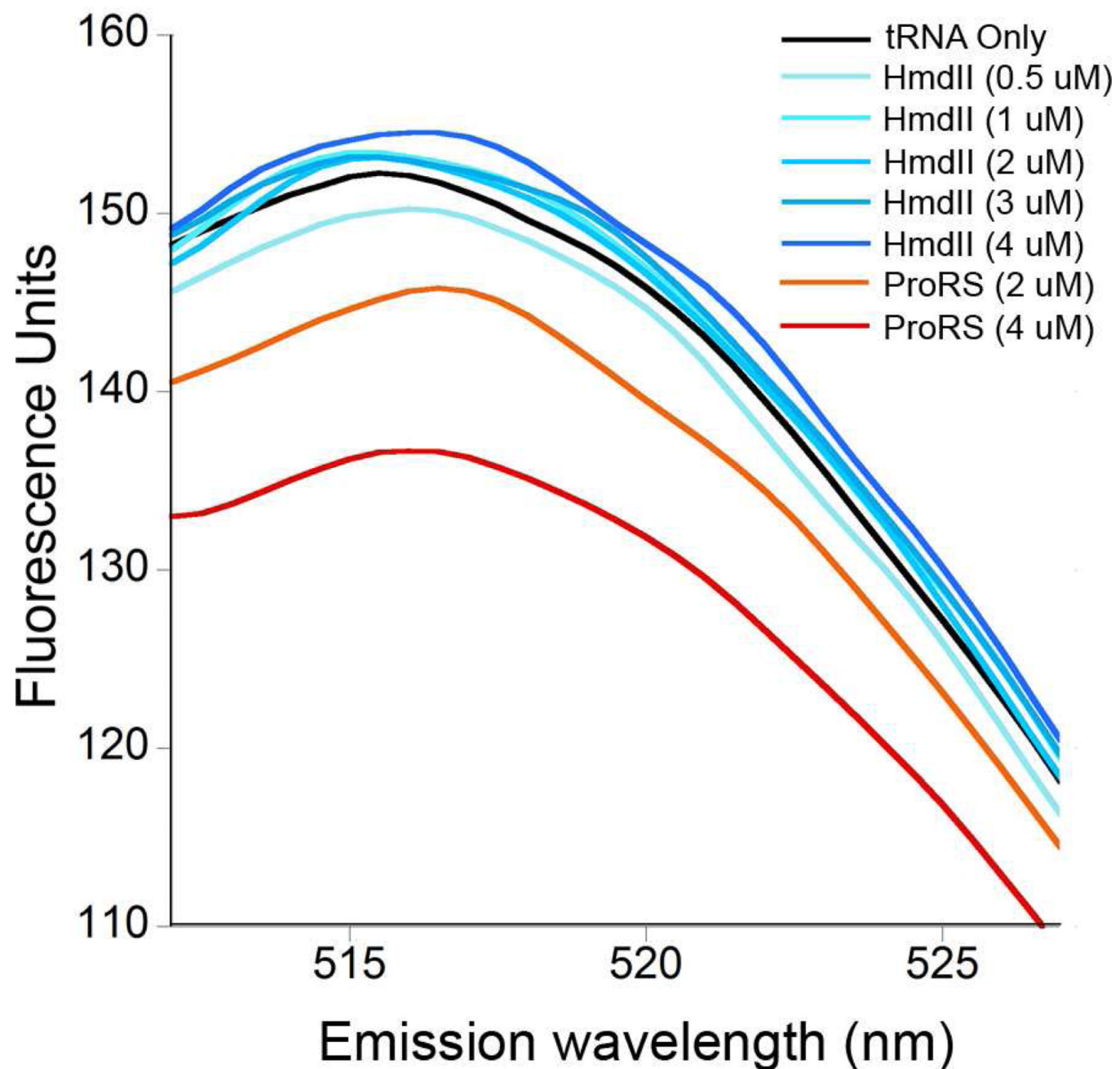
**Figure 4.**

Formation of protein-protein binary complexes measured by steady-state fluorescence anisotropy. ProRS is fluorescently labeled with Alexa Fluor 488 (F-ProRS) and monitored for changes in polarization upon the titration of tRNA<sup>Pro</sup> (A), Hmd (B), HmdII (C), or HmdIII (D).

**Figure 5.**

(A) Titration of Hmd into the preformed ProRS-tRNA<sup>Pro</sup> complex, observed by fluorescence anisotropy. The fluorescent label is present as 5'-fluorescein conjugated tRNA<sup>Pro</sup>. (B) EMSA for complex formation among ProRS, tRNA<sup>Pro</sup> and Hmd. While ProRS-tRNA<sup>Pro</sup> complex formation is observed, only a weak mobility shift of radiolabeled tRNA occurs for the Hmd binary complex. No change in the tRNA gel mobility shift generated by ProRS is observed upon further titration of Hmd. (C) Ternary complex formation for ProRS:tRNA<sup>Pro</sup>:HmdII observed by fluorescence polarization. The binding events are observed as ProRS (red circles) is first titrated into 5'-fluorescein conjugated tRNA<sup>Pro</sup>; a second binding event is observed upon further titration of HmdII (blue circles).

(D) Ternary complex formation observed by fluorescence polarization for ProRS:tRNA<sup>Pro</sup>:HmdIII depicted identically to panel (C). (E) Formation of the ProRS-tRNA<sup>Pro</sup>-HmdII ternary complex observed by EMSA. tRNA<sup>Pro</sup> is radiolabeled with <sup>32</sup>P as described in Methods. Supershifting upon addition of HmdII is evident. Similar data for HmdIII is not shown. (F) SDS PAGE gel of samples excised from the nondenaturing gel depicted in panel (E). Lanes A, B, C on this gel correspond to samples excised from the corresponding positions in the native gel shown in panel (E).

**Figure 6.**

Complex formation observed by steady-state fluorescence quenching. 5'- fluorescein conjugated tRNA<sup>Pro</sup> is used in these experiments. Titration of ProRS (red and orange traces) produces a significant quenching signal, while titration of HmdII does not.

7A

NIH-PA Author Manuscript NIH-PA Author Manuscript NIH-PA Author Manuscript NIH-PA Author Manuscript

Hmd	---MKIAILGAGCYRTHAAAGITNFMFACAEVAKEVGKPEIALTHSSITYGAELLHLVPDV	57
HmdII	MRNIRKIKVDNMKVSVYGAGNQNLINKLNLPFKFG-----GEPPYGGSRMAIE---	49
	::   : .   .: * . . : .   : : . . *   . . * . . * . : . :	
Hmd	KEVIVSDPCFAEFPGLVVIDEFDPKEVMEAHLSGNPESIMPKIREVVAKAKELIPKPPKA	117
HmdII	-----FAEAGHDVVLAEPN-KNIMSDDLWKK-----	74
	***   **: * : * : * . . * :	
Hmd	C <sub>1</sub> HLVHPE DVGLKVTSDREAVEGADIVITWLPGNKQPD <sub>1</sub> IKKFADAIPEGAIIVTHACT	177
HmdII	-----VEDAG <sub>1</sub> VKVSD <sub>1</sub> DVEAAKHGEIHLVLETPFGKATFR <sub>1</sub> IAKTIIEHVPEAVICNTCT	128
	**.**:***.*** **.. . : * : : * * :   * * .. : : * . . : : * . . : : * :	
Hmd	IPTTKFAKIEFKDLG---REDLNITSYHPGCVP-----EMKGQVYIAEGYASEEAVNK	226
HmdII	VSPVVLYYSLEPILRTKRKDVG <sub>1</sub> SSMHPAAVPGTPQHGHYVIGGKTTDGKELATEEQIKK	188
	: . . :   : . :   *: . . * : * . . * . . : * . . : * : * . . : :	
Hmd	LYEIGKIARGKAFKMPANLIGPVCDMCSAVTATVYAGLLAYRDAVTKILGAPADFAQMMA	286
HmdII	AVELAKSAGKEAYVVPADVSSVADMGSLVTAVALSGVLDYYTVGRKIINAPKKMIEQQV	248
	* . . * . . * : * . . * . . * . . * . . * . . * . . * . . * . . . . . .	
Hmd	DEALTQIHNL <sub>1</sub> MKEKGIANMEEALDPAALLGTADSMCFGPLAEILETALKVLEKHKVVEEE	346
HmdII	IMTLQTMASLVETSGIEGMVKALNPELLRSASSMKLLDRQKDLDAALEILQNLDETLKA	308
	: * . . * . . * . . * . . * . . * . . * . . * . . * . . * . . . . . .	
HmdI	GTKCEIMSQKE-----	358
HmdII	EVEKAEIKPTTLVAAQSLVKEIKTLIGGAAAEGAIKRSARKLFEH	353
	**	

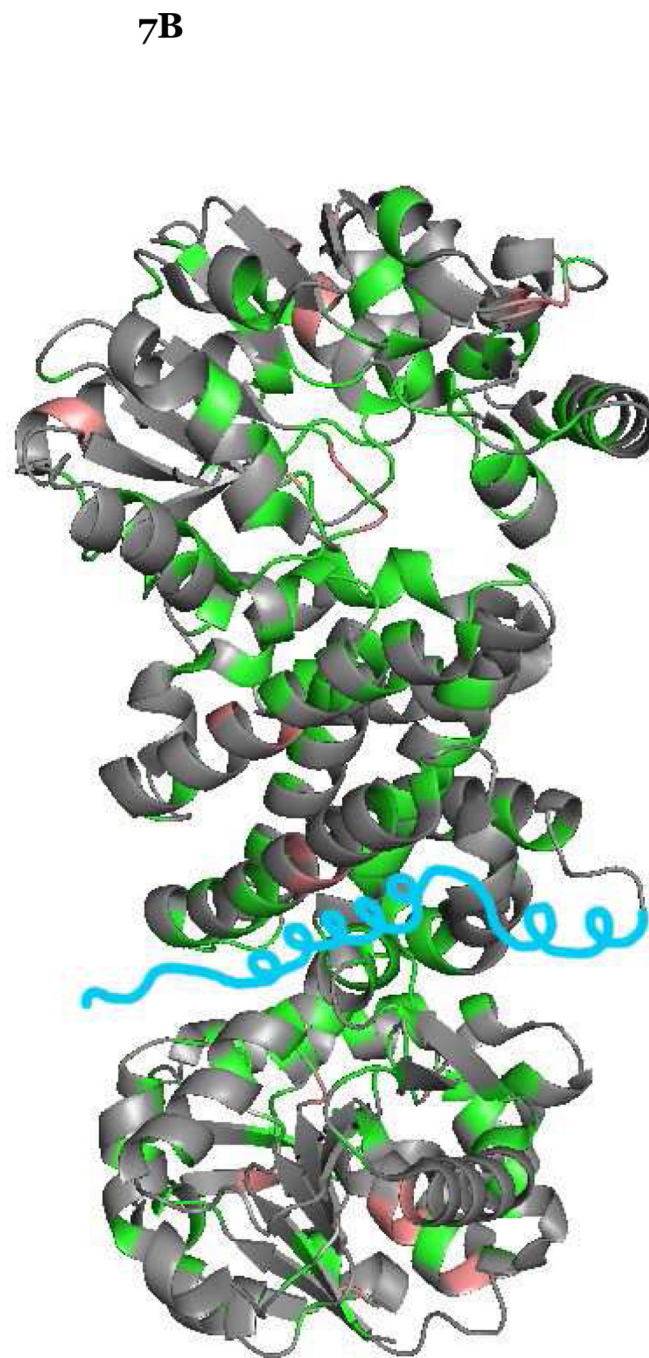


**Figure 7.**

(A) Sequence alignment of *Mj* Hmd and *Mj* HmdII. Amino acids that are conserved among the HmdII and HmdIII paralogs from all hydrogenotrophic methanogens are shaded in orange, while those conserved among all active Hmd enzymes are shaded in green. Basic residues found in the C-terminal extension that is unique to the paralogs, and that are conserved in over 75% of paralog sequences, are highlighted in blue. In this alignment of *Mj* Hmd sequences, a sixth basic residue (not highlighted) is present that is conserved in 50% of the other HmdII and HmdIII sequences. (B) Crystal structure of Hmd (RCSB code 3DAG).<sup>21</sup> Amino acids highlighted in panel (A) that are unique to the paralogs or to active Hmd enzymes are displayed in orange and green, respectively, on the tertiary structure. A

depiction of the C-terminal peptide for illustrative purposes is shown in light blue. The position of this peptide with respect to the remainder of the enzyme structure has not been modeled. The peptide is shown containing two  $\alpha$ -helices for consistency with earlier structure predictions.<sup>20,24</sup>

**Table 1**

Size exclusion chromatography

protein	Observed MW (kDa)	Theoretical MW (kDa) <sup>a</sup>	% Error	Oligomerization	Peak <sup>b</sup>
ProRS	113.3 335.1	56.78	0.2 1.7	Dimer Hexamer	C A
Hmd	82.95 117.9	41.21	0.6 4.8	Dimer Trimer	D
HmdII	75.25	38.35	1.9	Dimer	E
HmdIII	78.45 145.5	39.37	0.4 8.2	Dimer Tetramer	E B
tRNA <sub>Pro</sub>	25.26	25.04	0.9	Monomer	

<sup>a</sup>Theoretical molecular weight per monomer is computed from the amino acid sequence.<sup>b</sup>Peaks are denoted in Figure 1.

**Table 2**

tRNA binding affinities of Hmd and Hmd paralogs

	Hmd	HmdII	HmdIII
tRNA	K <sub>d</sub> (μM)	K <sub>d</sub> (μM)	K <sub>d</sub> (μM)
Asp <sup>a</sup>	>45	2.6 ±0.4	8.6 ±0.4
Cys <sup>a</sup>	26.5 ±0.3	2.3 ±0.2	10.0 ±0.2
Leu <sup>a</sup>	18.5 ±3.0	2.0 ±0.6	5.6 ±0.6
Lys <sup>a</sup>	40.8 ±0.7	6.3 ±0.2	18.3 ±0.2
Pro <sup>a</sup>	15.8 ±2.5	1.9 ±0.1	11.6 ±0.1
Pro <sup>b</sup>	>20	1.6 ±0.6	1.5 ±0.5

<sup>a</sup>Measured by EMSA.<sup>b</sup>Measured by fluorescence polarization

**Table 3**

Affinities of protein-protein complexes

	K <sub>d</sub> (μM)
AF <sup>a</sup> -ProRS:Hmd	2.10 ±0.31
AF-ProRS:HmdII	1.69 ±0.25
AF-ProRS:HmdIII	1.89 ±0.39

<sup>a</sup> AF denotes Alexafluor

**Table 4**

ATP-pyrophosphate exchange kinetics

Enzyme	$k_{cat}$ (sec <sup>-1</sup> )	$K_m$ [proline] (mM)	$k_{cat}/K_m$ (mM <sup>-1</sup> sec <sup>-1</sup> )
ProRS	2.1 ± 0.1	0.067 ± 0.013	31.6
ProRS/Hmd	3.6 ± 0.1	0.16 ± 0.024	22.2
ProRS/HmdII	4.0 ± 0.1	0.10 ± 0.006	40.5
ProRS/HmdIII	3.9 ± 0.1	0.11 ± 0.008	35.1